

Domain walls seeding the electroweak phase transition

Simone Blasi^{1,*} and Alberto Mariotti^{1,†}

¹*Theoretische Natuurkunde and IIHE/ELEM, Vrije Universiteit Brussel,
& The International Solvay Institutes, Pleinlaan 2, B-1050 Brussels, Belgium*

Topological defects can act as local impurities that seed cosmological phase transitions. In this paper we study the case of domain walls, and how they can affect the electroweak phase transition in the Standard Model extended with a Z_2 -odd scalar singlet. When the transition is two-step, the early breaking of the Z_2 symmetry implies the formation of domain walls which can then act as nucleation sites for the second step. We develop a method based on dimensional reduction to calculate the rate of the catalyzed phase transition within the 3d theory on the domain wall surface. By comparison with the standard homogeneous rate, we conclude that the seeded phase transition is generically faster and it ultimately determines the way the phase transition is completed. We comment on the phenomenological implications for gravitational waves and baryogenesis.

CONTENTS

I. Introduction	1
II. Seeded vs homogeneous vacuum decay	2
III. The SM plus scalar singlet	3
IV. Formalism for the seeded phase transition	4
A. Kaluza–Klein decomposition	4
B. Thin wall approximation	7
V. Results	9
A. The rolling	9
B. The tunneling	11
C. The bubble	12
VI. Discussion	13
Acknowledgements	14
A. Bubble tension in the thin wall approximation	14
B. Estimate of the nucleation temperature	15
References	15

I. INTRODUCTION

The study of cosmological phase transitions is of great importance in high energy physics as it can shed light on major open questions in the Standard Model (SM), such as the origin of the matter–anti matter asymmetry in the Universe, and can help us uncovering the dynamics of the electroweak symmetry breaking thanks to the exciting prospects for detecting the corresponding background of gravitational waves in the near future [1, 2].

The physics of first order phase transitions crucially depends on the mechanism controlling the bubble nucleation. This is usually assumed to proceed via thermal or quantum fluctuations in a homogeneous spacetime. There is, however, the possibility that impurities that are present in the Universe at the time of the phase transition can actually seed the bubble nucleation, thus providing a competing mechanism to complete the phase transition [3–7]. Following [3], we will refer to the first case as homogeneous nucleation, and to the second case as inhomogeneous or seeded nucleation, since in the latter the tunneling probability is not uniformly distributed on the spacetime, but it is enhanced at the location of the seeds.

The nature of the impurities can be vastly different, ranging from black holes [8–13] and local overdensities [14, 15], to topological defects [3–5, 7, 16–27], with also possible implications for the lifetime of the metastable SM vacuum [28–30]. Concerning phase transitions seeded by topological defects, previous studies have mostly focussed on cosmic strings [16, 17, 19–21, 25] and monopoles [3, 22, 23, 27].

In this paper we investigate the case of domain walls, topologically stable two-dimensional objects forming at the spontaneous breakdown of a discrete symmetry [31, 32]. In particular, we will focus on two-step phase transitions where the defects created in the first step can act as seeds for the second one. As a primary case of study, we consider the possibility that domain walls have played a role in the electroweak phase transition.

As a matter of fact, probably the simplest physics beyond the SM that can turn the electroweak crossover into a first order phase transition is the addition of a real scalar field, S , singlet under the SM gauge group [33–51]. Since our focus is the role of domain walls, we will be interested in the case in which S is odd under a Z_2 symmetry. This scenario actually implies a very minimal set of new physics effects, given that any mixing between the Higgs and the singlet is suppressed, and it has been studied extensively at present and future colliders [43–45, 49, 52, 53].

A typical way in which the phase transition can proceed in this scenario is indeed by a two-step process in

* simone.blasi@vub.be

† alberto.mariotti@vub.be

which first the singlet S develops a non-zero vacuum expectation value (vev), and a second step (which is usually first order) leading to the breakdown of the electroweak symmetry. Given that the singlet is odd under a Z_2 , the first step will lead to the formation of domains whose vacua are related by this symmetry, with walls forming at their boundaries according to the Kibble mechanism [32].

These domain walls are however not cosmologically stable if the actual vacuum of the theory entails a vanishing singlet vev, so that the Z_2 symmetry is eventually restored at the end of the electroweak phase transition, as also noted in Ref. [54]. This means that domain walls can act as seeds for the phase transition while being collapsed upon its completion.

The purpose of this paper is to study the details of this process. As we shall see, domain walls can catalyze the electroweak phase transition in two ways, namely either by developing a classical instability and dissociating, or by acting as nucleation sites favoring the quantum/thermal tunneling. In order to calculate the rate of this tunneling we will develop a formalism based on a Kaluza-Klein reduction technique, which could in principle be extended to study other defects as well. We will also present a complementary approach based on the thin-wall approximation to gain further intuition on this inhomogeneous nucleation.

In the parameter space that we have covered for the Higgs-singlet model, we find that the inhomogeneous transition is always faster than the homogeneous one. Moreover, regions of parameter space in which bubbles would fail to nucleate according to the standard tunnelling rate can now become viable thanks to the domain walls—see Fig. 3 for an overview of our results. This can largely affect the phenomenological properties of the electroweak phase transition, such as for instance its duration and the geometry of the nucleated bubbles with implications for the gravitational wave signal, as discussed in Sec. VI. together with interesting future directions.

II. SEEDED VS HOMOGENEOUS VACUUM DECAY

The phase transition seeded by domain walls can proceed via two mechanisms:

- domain walls can become classically unstable while the Universe cools down, developing a region of the true vacuum in their interior, and then dissociate;
- even if an instability never develops, domain walls can nevertheless facilitate the tunneling towards the true vacuum by acting as local impurities.

Both these possibilities, dubbed *Rolling* and *Tunneling*, respectively, can be described in the dimensionally-reduced theory presented in Sec. IV.

In order to first understand in generality the dynamics of the seeded tunneling, we here revisit the computation

of the nucleation condition for the homogeneous phase transition and compare it with the one derived when domain walls act as nucleation sites.

The rate of false vacuum decay per unit volume for a homogeneous tunneling can be written as [55–57]

$$\gamma_V \equiv \frac{\Gamma}{V} = A \exp(-S_3/T), \quad (1)$$

where S_3 is the time-independent euclidean action evaluated on the $O(3)$ symmetric bounce solution, and the prefactor can be estimated as $A \sim T^4$. In order to determine the nucleation temperature, T_n , at which the phase transition actually takes place in an expanding Universe, one needs to impose (see e.g. [58])

$$\mathcal{N}(T_n) = \int_{T_n}^{T_c} \frac{\gamma_V}{H^4} \frac{dT}{T} = 1 \quad (2)$$

where \mathcal{N} is the number of bubbles nucleated inside one Hubble volume, H^{-3} , in the range between the critical temperature, T_c , and T_n . The integral for \mathcal{N} is typically dominated by temperatures around T_n . Moreover, with the notable exception of strongly supercooled phase transitions, we can assume radiation domination throughout the whole nucleation process. This leads to the standard condition

$$\frac{S_3(T_n)}{T_n} \simeq 4 \log(M_{\text{Pl}}/T_n) - 11.4 \approx 145, \quad (3)$$

where in the last step we have set T_n around the electroweak scale, and M_{Pl} is the Planck mass.

Let us now move to discuss the case of a tunneling process than can only occur in the vicinity of an impurity, which we shall take to be a domain wall. It is then natural to define a nucleation rate per unit surface given by [18, 19]

$$\gamma_S \equiv \frac{\Gamma}{S} = A' \exp(-S_{\text{inh}}) \quad (4)$$

where $A' \sim \sigma_{\text{DW}}$ is the tension of the domain wall and S_{inh} is the action describing the inhomogeneous tunneling. In order to evaluate the nucleation condition we parameterize the total surface occupied by domain walls inside one Hubble volume as $S_H = \xi H^{-2}$, where ξ is $\mathcal{O}(1)$ in the scaling regime [59]. The new condition then reads

$$\mathcal{N}(T_n) = \int_{T_n}^{T_c} \xi \frac{\gamma_S}{H^3} \frac{dT}{T} = 1 \quad (5)$$

and therefore

$$S_{\text{inh}} = 3 \log(M_{\text{Pl}}/T_n) + \log(\sigma_{\text{DW}}/T_n^3) + \log \xi - 8.5 \approx 105 \quad (6)$$

for a transition around the electroweak scale, where we have assumed in addition that also the tension of the domain wall is set by the electroweak scale, as this will be the focus of our study.

The bounce action S_{inh} is associated with the formation of a bubble that modifies the original domain wall profile, and that also extends in the z direction orthogonal to it. Its geometry will then deviate from the $O(3)$ spherical symmetry at high temperatures, but it will preserve the $O(2)$ rotational invariance in the plane parallel to the domain wall described by r . As we shall see in Sec. V C, the shape of the bubble may then resemble the one of a spheroid nucleated inside the domain wall.

The euclidean action setting the tunneling rate can be computed once the field profiles corresponding to the bounce solution are known. In the case of a tunneling seeded by domain walls, we may then search for a high-temperature solution for the fields Φ_i involved in the tunneling process, $\Phi_i = (S, h)$ for the Higgs-singlet model, that is independent of the euclidean time, $\Phi_i(r, z)$. The boundary conditions will be such that the unperturbed domain wall is recovered for $r \rightarrow \infty$ and $z \rightarrow \pm\infty$, together with $\partial_r \Phi_i(r = 0, z) = 0$. The bounce action at the temperature T will then be given in this case by $S_{\text{inh}} = S_2/T$, where the subscript refers to the $O(2)$ symmetry of the solution.

This solution may be obtained by solving the coupled system of partial differential equations with the aforementioned boundary conditions. In Sec. IV A we will instead introduce a new approach based on a Kaluza-Klein (KK) decomposition along the direction orthogonal to the domain wall. As we shall see, this provides an alternative way of computing the bounce action (and hence the transition rate), and at the same time gives a more physical picture of the inhomogeneous tunneling.

III. THE SM PLUS SCALAR SINGLET

Before introducing the formalism needed to describe the seeded phase transition, we shall here introduce our case of study, namely the SM extended with a real scalar singlet that is odd under a Z_2 symmetry. The potential at the renormalizable level in the unitary gauge reads

$$V(h, S) = -\frac{\mu^2}{2}h^2 + \frac{\lambda}{4}h^4 - \frac{m^2}{2}S^2 + \frac{\eta}{4}S^4 + \frac{\kappa}{2}h^2S^2, \quad (7)$$

where the Higgs component h is such that $\mathcal{H} = (0, h)/\sqrt{2}$, and we shall take $\kappa > 0$ and $\mu^2, m^2 > 0$. The parameter m^2 can be traded for the physical singlet mass in the $(h = v, S = 0)$ vacuum at zero temperature, m_S^2 , as

$$m^2 = \kappa v^2 - m_S^2. \quad (8)$$

Since our focus is the seeded vacuum decay, we will only consider the case in which the electroweak phase transition occurs in two steps, as we shall briefly discuss. Assuming that the vacuum at high temperatures corresponds to vanishing h and S so that all symmetries are “restored”, the first step entails the spontaneous breaking of the discrete Z_2 symmetry at the temperature T_d , with

the singlet scalar developing a non-vanishing vacuum expectation value (vev) $v_s = m/\sqrt{\eta}$, while the Higgs minimum is still at zero. At this point, given that $\langle S \rangle = \pm v_s$ are energetically equivalent configurations, regions with $+$ and $-$ will form inside a Hubble patch separated by domain walls at the boundaries, with profile given by

$$S_{\text{DW}}(z) = v_s \tanh(mz/\sqrt{2}). \quad (9)$$

At temperatures below the critical temperature, T_c , the $(0, \pm v_s)$ vacuum becomes metastable and decays to the (true) electroweak vacuum $(v, 0)$. The two-step phase transition can then be summarized as

$$(0, 0) \rightarrow (0, v_s) \rightarrow (v, 0). \quad (10)$$

The second step of the chain is usually assumed to occur in homogeneous spacetime, equivalently either inside the $+$ or $-$ domains, and it is typically first-order. However, if walls are present at the time of electroweak symmetry breaking they can induce a seeded vacuum decay that can only take place close to the boundary between the domains. In fact, at the center of the domain wall, $z = 0$ in (9), the singlet vev is vanishing, and so would be the barrier to reach the true vacuum according to the potential in (7). Even though an actual barrier still exists due to the non-zero gradient of the domain wall profile, this argument gives an intuitive understanding of how the phase transition can be facilitated by the domain walls. This process then provides a competing mechanism for the second step in (10), since homogeneous tunneling can of course still occur far away from the domain walls.

In order to have a seeded vacuum decay, domain walls formed at T_d need not to collapse before the electroweak phase transition has completed. This aspect is connected to the quality of the corresponding discrete symmetry. In fact, the effect of small Z_2 -breaking terms in the scalar potential (7) is to induce a bias ϵ between the two minima at $\pm v_s$, which acts as a vacuum pressure that tends to expand the domain corresponding to the deepest minimum over the other until the domain structure is destroyed. This collapse can of course be prevented by the domain wall tension. However, if the characteristic scale of the network (and hence the curvature radius) is of order H^{-1} as eventually expected in the scaling regime, the collapse will be almost instantaneous after formation, unless the energy difference ϵ is extremely small, see e.g. [54, 60]. In practice, this means that the Z_2 needs to be exact for all the operators up to dimension four.

On the other hand, no “special” quality for the Z_2 symmetry is required if its breaking is due to gravity. In fact, even if this breaking is generated already at dimension five with an operator S^5/Λ , domain walls can still play a role in the electroweak phase transition if the cutoff Λ is at the Planck scale and $v_s \sim 100$ GeV [60]. Indeed the domain wall annihilation temperature, T_{ann} , can be estimated by requiring that the tension force σ_{DW}/R (where $\sigma_{\text{DW}} \sim \eta^{1/2}v_s^3$ is the domain wall tension and $R \sim 1/\xi H$

is the typical curvature radius) equals the vacuum pressure due to the bias, $\epsilon \sim c v_s^5 / M_{\text{Pl}}$ with c a $\mathcal{O}(1)$ coefficient. We then obtain

$$\frac{T_{\text{ann}}}{v_s} \sim 0.5 \frac{c^{1/2}}{\xi^{1/2} \eta^{1/4}}, \quad (11)$$

where the Planck scale drops out from the calculation as this sets both the typical curvature radius through Hubble and the size of the bias. We then conclude that a Z_2 explicit breaking due to gravity is generically not enough to make the domain walls collapse before the electroweak phase transition, as T_{ann} in (11) can easily be below the nucleation temperature.

We nevertheless note that the model can have a viable phenomenology also with an exact Z_2 symmetry: even though scalar singlet dark matter with large portal coupling to the Higgs boson is almost excluded for the mass range of interest, S needs not to be the lightest state charged under this symmetry. In addition, domain walls are anyways collapsed at the end of the electroweak phase transition ensuring no contradiction with standard cosmology.

IV. FORMALISM FOR THE SEEDED PHASE TRANSITION

The seeded phase transition can be described as a process in which the unperturbed domain wall is modified by the onset of a Higgs vev at its core eventually filling up the whole space. As mentioned in Sec. II, this can occur either via a classical instability of the unperturbed domain wall profile (rolling), or, if this configuration is metastable, via thermal or quantum tunneling.

Both these scenarios can be captured by analyzing the lower-dimensional effective theory obtained by performing a KK decomposition along the direction orthogonal to the domain wall. This strategy is discussed in Sec. IV A. In addition, we can gain further physical intuition by resorting to a thin wall approximation in which the role of the pre-existing domain wall becomes manifest in facilitating the tunneling to the true vacuum. This will be the topic of Sec. IV B.

Interestingly, these two formalisms can actually describe the tunneling process in complementary temperature ranges, namely far from T_c (KK decomposition), and close to T_c (thin wall), as we shall discuss in detail in Sec. V.

A. Kaluza–Klein decomposition

The starting point is to make an ansatz for the singlet and the Higgs field in the background of the unperturbed domain wall as

$$S = S_{\text{DW}}(z) + \sum_k s_k(x) \sigma_k(z), \quad h = \sum_k h_k(x) \phi_k(z) \quad (12)$$

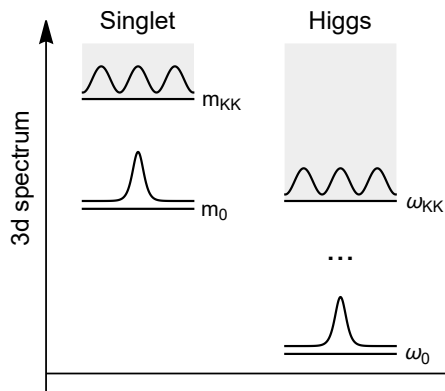


Figure 1. A cartoon of the spectrum of the 3d theory according to the eigenvalue equations (13) and (14). The singlet modes consist of a single bound state (neglecting the massless mode from the breaking of translational invariance) with mass $m_0^2 > 0$ indicated by the solid line, together with a sketch of its localized profile. On top of this there is a gapped continuum of KK states shown by the upper gray region, with plane-wave asymptotic behaviour. The Higgs spectrum is qualitatively the same besides the fact that more discrete modes can in principle be present, and that the mass of the lightest state ω_0^2 needs not to be positive.

where $S_{\text{DW}}(z)$ is the profile given in Eq. (9), which is a solution to the equations of motion together with $h = 0$, and we have denoted by x the remaining three space-time coordinates. The sum runs over a complete set of eigenfunctions, $\sigma_k(z)$ and $\phi_k(z)$. The ansatz (12) can be plugged into the 4d action of the Higgs–singlet model in order to obtain a theory for the 3d modes $s_k(x)$ and $h_k(x)$, which will allow us to study the occurrence of classical instabilities, and furthermore to calculate the seeded tunneling rate as a standard homogeneous process in three spacetime dimensions.

The 4d potential (7) is of course temperature dependent. This means that in principle a new decomposition needs to be performed at each temperature of interest. As we shall see, however, in some limits such as the leading high temperature expansion this is not necessary. We will then first present our procedure at $T = 0$ and then discuss a simple way to extend it at finite temperature.

In order to diagonalize the quadratic part of the 3d action, the profiles σ_k and ϕ_k are taken to be solutions to the eigenvalue equations

$$-\sigma_k'' + (3\eta S_{\text{DW}}^2(z) - m^2)\sigma_k = m_k^2 \sigma_k, \quad (13)$$

$$-\phi_k'' + (\kappa S_{\text{DW}}^2(z) - \mu^2)\phi_k = \omega_k^2 \phi_k, \quad (14)$$

which correspond to a Pösch–Teller potential and can be solved exactly in terms of Legendre polynomials. A cartoon of the spectrum for the Higgs and singlet states is shown in Fig. 1.

The singlet spectrum consists of a discrete mode, σ_0 , corresponding to a bound state, and a tower of scattering states, σ_k , with plane-wave asymptotic behaviour. The

corresponding masses are given by (see e.g. [61])

$$m_0^2 = \frac{3}{2}m^2, \quad m_k^2 = \left(\frac{q_k^2}{2} + 2 \right) m^2 \quad (15)$$

and we have neglected the massless mode associated to the breaking of translational invariance as it will play no role in what follows. Here $q_k > 0$ denote the dimensionless wavevectors of the continuum states which for concreteness we can consider normalized in a box of size $z \in (-L, L)$. The corresponding eigenfunctions read

$$\sigma_0(z) \propto \frac{\tanh(bz)}{\cosh(bz)}, \quad (16)$$

$$\sigma_k(z) \propto e^{iq_k bz} (3 \tanh^2(bz) - 1 - q_k^2 - 3iq_k \tanh(bz)),$$

where we have introduced $b = m/\sqrt{2}$.

The spectrum of the Higgs states is qualitatively the same. It consists of n discrete modes (bound states) with masses ω_n^2 given by

$$\omega_n^2 = \frac{m^2}{2} (p + 2np - n^2) - \mu^2, \quad (17)$$

where $n = p - \nu$ with $p(p+1)/2 = \kappa/\eta$, namely

$$p = \frac{1}{2} \left(\sqrt{1 + \frac{8\kappa}{\eta}} - 1 \right). \quad (18)$$

The allowed values for ν are

$$0 < \nu = p, p-1, p-2, \dots \quad (19)$$

and the localized profiles are given by

$$\phi_n(z) \propto (1-x^2)^{-\nu/2} \frac{d^n}{dx^n} (1-x^2)^p \Big|_{x=\tanh \frac{mz}{\sqrt{2}}}, \quad (20)$$

with $\mathcal{O}(m^{-1})$ spread around $z = 0$. When n is zero or even, the profile will be symmetric for $z \rightarrow -z$, and antisymmetric otherwise. The lightest discrete mode corresponds to $n = 0$.

On top of the bound states, there will be a gapped continuum in the Higgs decomposition as well, starting at $\omega_{\text{KK}}^2 > \kappa v_s^2 - \mu^2$ with definite parity. The masses of the continuum states are then given by

$$\omega_k^2 = \left(\frac{\tilde{\nu}_k^2}{2} + \frac{\kappa}{\eta} \right) m^2 - \mu^2, \quad (21)$$

where $\tilde{\nu}_k$ is a dimensionless wavevector similarly to q_k in (15). The even continuum profiles ϕ_k^e are given by

$$\phi_k^e(z) \propto \text{Im} \left\{ (1+p+i\tilde{\nu}_k) P_{p+1}^{-i\tilde{\nu}_k}(0) P_p^{i\tilde{\nu}_k}(\tanh bz) \right\}. \quad (22)$$

Far from the domain wall they approach a plane wave form,

$$\phi_k^e(z \rightarrow \infty) \propto \text{Im} \left\{ \frac{(1+p+i\tilde{\nu}_k) P_{p+1}^{-i\tilde{\nu}_k}(0)}{\Gamma(1-i\tilde{\nu}_k)} e^{i\tilde{\nu}_k bz} \right\}. \quad (23)$$

The allowed values for $\tilde{\nu}_k > 0$ are again dictated by the boundary conditions in the box $z \in (-L, L)$, which we shall take to be $\phi_k^e(L) = 0$, and they merge into a continuum for $L \rightarrow \infty$.

For completeness we present the odd solutions ϕ_k^o as well,

$$\phi_k^o(z) \propto \text{Im} \left\{ P_p^{i\tilde{\nu}_k}(0) P_p^{-i\tilde{\nu}_k}(\tanh bz) \right\}, \quad (24)$$

with a similar plane-wave asymptotic behaviour.

Plugging the decomposition above into the 4d action, we obtain the quadratic part of the 3d theory,

$$S^{(2)} = \int d^3x \left[\frac{1}{2} (\partial_\mu h_k)^2 + \frac{1}{2} (\partial_\mu s_k)^2 - \frac{\omega_k^2}{2} h_k^2 - \frac{m_k^2}{2} s_k^2 \right], \quad (25)$$

where the implicit sum over k runs over both the discrete and the continuum modes.

The interacting part of the 3d theory can be obtained from the 4d potential V by performing the various overlap integrals in the z direction. This will generate a 3d potential \tilde{V} with trilinear and quadrilinear terms in the fields. Restricting ourselves for a moment to the lowest-lying discrete states h_0 and s_0 , we have

$$\begin{aligned} \tilde{V} \supset & \frac{1}{4} (c_\lambda m) \lambda h_0^4 + (c_{3\eta} m^{3/2}) \sqrt{\eta} s_0^3 + \frac{1}{4} (c_{4\eta} m) \eta s_0^4 \\ & + (c_{3\kappa} m^{3/2}) \frac{\kappa}{\sqrt{\eta}} s_0 h_0^2 + \frac{1}{2} (c_{4\kappa} m) \kappa h_0^2 s_0^2, \end{aligned} \quad (26)$$

where the c coefficients are $\lesssim \mathcal{O}(1)$ numbers related to the relevant overlap integrals. For example, $c_{3\kappa}$ is given by

$$c_{3\kappa} \equiv m^{-3/2} \int_{-L}^L dz \sigma_0(z) \sqrt{\eta} S_{\text{DW}}(z) \phi_0^2(z), \quad (27)$$

and depends on the 4d couplings through the dimensionless combination κ/η . Similar interaction terms where h_0 and s_0 are replaced by continuum states will also appear in \tilde{V} alongside the ones shown in (26).

Since the true vacuum of the 4d theory will have $h = v$ everywhere, we expect only the even Higgs profiles to play a role in the phase transition. Similarly, the true vacuum corresponds to $S = 0$, so that only the odd singlet modes will be excited in order to (partly) cancel the unperturbed domain wall. In addition, we expect the seeded bubble to have a definite symmetry for $z \rightarrow -z$, which requires either the odd or the even modes to be identically zero for each field. In the following we shall therefore neglect the odd and even states for the Higgs and the singlet, respectively. From the point of view of the 3d theory, we can see that some overlap integrals for these modes will vanish, so that their vevs are expected to be set to zero dynamically when minimizing the potential, leading to the same conclusion.

Up to this point the 3d theory under consideration is equivalent to the 4d theory provided that all the continuum states are taken into account. This may be however not possible in practice, and in the following we shall discuss how the heavy KK states may be integrated out in favor of an effective theory for the lowest-lying modes. In particular, we will focus on the theory obtained by integrating out the two towers of continuum Higgs and singlet KK modes, thus keeping only h_0 and s_0 as dynamical¹. The reason for including s_0 in the effective theory despite its rather large mass is that we expect its vev to change more significantly with respect to the vevs of the continuum states, as this will be the leading correction to the unperturbed domain wall.

The two-field effective theory obtained in this way will consist of operators made of h_0 and s_0 up to the sixth power at the order $\mathcal{O}(1/m_{\text{KK}}^2)$, and even in h_0 . At the order $\mathcal{O}(1/m_{\text{KK}}^4)$ interactions are generated up to the eighth power together with momentum-dependent operators². All these new terms should then be added to the ones shown in (26).

We may estimate the condition for the validity of the effective theory in terms of the maximum size of the h_0 and s_0 vevs by requiring that the induced shift in the masses of the continuum modes remains a small correction. Considering the contribution from $h_0 \neq 0$ to all the singlet KK states, we can then require

$$\frac{\Delta m^2}{m_{\text{KK}}^2} \equiv \int_0^\infty \frac{dq}{\sqrt{2\pi}} \frac{c_{4\kappa}(q)m\kappa h_0^2}{(q^2/2 + 2)m^2} < 1 \quad (28)$$

where we have replaced the sum over the states in the box of size $2L$ with an integral over q_k . The coefficient $c_{4\kappa}(q)$ is the analogue of $c_{4\kappa}$ in (26) for the operator $h_0^2 s_k^2$, in which s_0 has now been replaced with states of the continuum tower. The integral (28) is dominated by the lightest KK states due to the $1/q^2$ suppression, so that we can write

$$\frac{\Delta m^2}{m_{\text{KK}}^2} = \frac{\bar{c}_{4\kappa}\kappa}{2\sqrt{2}m} h_0^2 \quad (29)$$

where we have defined $\bar{c}_{4\kappa} < 1/2$ as an average coupling, resulting in the condition

$$h_0^2 < \frac{2\sqrt{2}m}{\bar{c}_{4\kappa}\kappa}. \quad (30)$$

A similar result is obtained for s_0^2 by estimating the correction to the Higgs continuum masses. We thus

conclude that the 3d cutoff of the effective theory is set by the scale $\sim \sqrt{m/\kappa}$ up to a order-few factor. We will use this as an approximate criterium to assess the validity of the effective theory.

Let us now discuss how temperature corrections can be taken into account in this picture. In general, the terms arising from thermal loops cannot be fully reabsorbed into a redefinition of the tree level couplings in (7). However, in the leading high-temperature approximation in which only the terms $\propto T^2$ are retained, these effects can be captured with a simple redefinition of the scalar mass terms,

$$\mu^2 \rightarrow \mu^2 - c_h T^2, \quad m^2 \rightarrow m^2 - c_s T^2 \quad (31)$$

where c_h and c_s are given by [39]

$$c_h = \frac{2m_W^2 + m_Z^2 + m_h^2 + 2m_t^2}{4v^2} + \frac{\kappa}{12}, \quad c_s = \frac{4\kappa + 3\eta}{12}. \quad (32)$$

The procedure outlined above can be promoted at finite temperature in a straightforward way by replacing the bare masses in (7) with their temperature corrected values. This also implies that a change in the temperature can be accounted for by a simple shift in all the 3d masses in (25). In addition, if the coordinates are measured in units of $1/m(T)$ the interaction Lagrangian can actually be kept constant with T . In practice this means that it is not necessary to perform the full KK reduction whenever the temperature is modified.

We note that beyond the high temperature approximation at order T^2 the profile of the domain wall will, in general, no longer respect the functional form in (9) so that the 3d eigensystem may be found only numerically, challenging the feasibility of our procedure. On the other hand, the additional terms in the thermal potential that involve only the Higgs field can in principle be added without spoiling the exact solution of the eigensystem, with the effect of introducing more interactions in the 3d potential. For simplicity we shall however stick to the high temperature approximation at order T^2 in what follows, and neglect in addition loop corrections to the potential (7) as we do not expect these to change the conclusions of our analysis.

Within these assumptions, we can now study the thermal history of the SM plus singlet model from the point of view of its 3d description and identify the two cases of rolling and tunneling mentioned in Sec. II. These two different scenarios can be distinguished by looking at the sign of ω_0^2 from (17) at different temperatures,

$$\omega_0^2(T) = \frac{1}{2}p(m^2 - c_s T^2) - \mu^2 + c_h T^2. \quad (33)$$

Since by assumption the electroweak symmetry is still unbroken at the temperature T_d (corresponding to the Z_2 breaking), we will have $c_h T_d^2 - \mu^2 > 0$ and thus $\omega_0^2(T_d)$

¹ In fact, the relevant parameter space will be such that $p < 1$, so that there will be a single Higgs bound state with $n = 0$ and $\nu = p$. If present, additional bound states can nonetheless be included straightforwardly.

² We generically indicate by m_{KK} the mass scale of the continuum modes for both the Higgs and the singlet towers.

is positive right after the formation of the domain walls. This means that the 3d potential will have a global minimum with all the vevs set to zero.

If then $\omega_0^2(T)$ turns negative for $T_d > T > T_c$, the domain wall will become classically unstable and roll towards a more favorable configuration with a non-vanishing Higgs profile inside the domain wall, in close analogy with the bosonic realization of string superconductivity [62]. Finding this configuration corresponds to minimize the 3d potential \tilde{V} in terms of the vevs of the discrete and continuum modes. When the temperature drops below the critical temperature, the true vacuum of the theory is the electroweak one where $S = 0$, and we then expect this 3d minimum to turn unstable and the domain wall to dissociate. This case will be discussed in more detail in Sec. V A.

The other possibility is that the Higgs eigenvalue $\omega_0^2(T)$ may turn negative only at $T < T_c$, or actually stay positive even at zero temperature. Considering the effective theory where the KK towers are integrated out, this means that the origin in the (h_0, s_0) plane, where $\tilde{V} = 0$, is a local minimum. The actual location of the global minimum is instead beyond the capability of the effective theory: this is because the configuration with $h(x, z) = v$ and $S(x, z) = 0$ corresponds in the 3d picture to the whole tower of KK states taking non-negligible vevs. Nonetheless, if the 3d potential turns negative for field values close to the origin, the seeded false vacuum decay can be studied as a standard tunneling process

$$(0, 0)_{3d} \rightarrow (\langle h_0 \rangle, \langle s_0 \rangle)_{3d}, \quad (34)$$

provided that the release point is within the validity of the effective theory³. Having calculated the release point in terms of h_0 and s_0 , the actual profile of the 4d seeded bubble can be reconstructed through the KK decomposition in (12), where the vevs of the continuum states are fixed by their equations of motion that we have used to integrate them out.

The tunneling process (34) can be solved with usual techniques. In the high temperature limit, it consists of finding a time-independent solution with $O(2)$ symmetry to the system of ordinary differential equations

$$\phi_i'' + \frac{1}{r} \phi_i' = \frac{\partial \tilde{V}}{\partial \phi_i}, \quad \phi_i = h_0, s_0 \quad (35)$$

which can be solved e.g. with `CosmoTransitions` [63], with $r^2 = x^2 + y^2$ being the radius in the domain wall

plane, and boundary conditions $\phi_i(\infty) = 0$ and $\phi_i'(0) = 0$ ensuring that the unperturbed domain wall is recovered at $r = \infty$. The bounce action corresponding to this solution will be indicated by S_2/T , where the suffix refers to the $O(2)$ symmetry, and will be studied in detail in Sec. V B and V C.

The same strategy may be applied to search for solutions with a spherical symmetry $O(3)$ involving the radial variable on the domain wall and the euclidean time τ ,

$$\phi_i'' + \frac{2}{\rho} \phi_i' = \frac{\partial \tilde{V}}{\partial \phi_i}, \quad \phi_i = h_0, s_0 \quad (36)$$

where $\rho^2 = r^2 + \tau^2$, which can be solved with help of `CosmoTransitions` and `FindBounce` [64]. The corresponding \tilde{S}_3 action, where the suffix refers to the $O(3)$ symmetry, is expected to become smaller than S_2/T only at very low temperatures and will play no role in our analysis, as domain walls are anyway destroyed at the time of the electroweak phase transition. Let us however note that \tilde{S}_3 can be relevant in different scenarios where the defects survive until today and may then affect the SM life time.

Let us now briefly discuss how the boundary conditions for the bounce along z are satisfied in the approach discussed above. These conditions are such that the false vacuum $(0, \pm v_s)$ needs to be recovered at $z \rightarrow \pm\infty$. As far as the discrete modes h_0 and s_0 are concerned, this is automatically the case because the localized profiles $\phi_0(z)$ and $\sigma_0(z)$ vanish at $|z| = \infty$. On the other hand, scattering states will oscillate with a certain amplitude far away from the domain wall, and only an infinite superposition may lead to the exact boundary condition. However, already the individual amplitude of these oscillations is expected to be small given that they are suppressed by the KK scale, so that no additional condition needs to be imposed besides the validity of the effective theory.

Finally, let us mention that there is one caveat to this procedure when applied to the effective theory at $\mathcal{O}(1/m_{\text{KK}}^4)$ due to the occurrence of momentum-dependent operators. These would in fact modify the equations of motion (35) and (36) beyond a simple change in the shape of the potential \tilde{V} , which would then require a non-trivial modification of the solving procedure. In our analysis we will neglect the derivative operators when evaluating S_2/T at $\mathcal{O}(1/m_{\text{KK}}^4)$ and leave this improvement for future work.

B. Thin wall approximation

In this section we shall discuss an alternative approach, namely the thin wall (TW) approximation, to calculate the inhomogeneous tunneling rate induced by the domain walls. While the TW approximation has limited validity for what concerns the temperature range, it has the virtue of providing further insights in the physics of the

³ For consistency, we also need to require that the size of the bubble nucleated inside the domain wall is smaller than the correlation length of the network, such that the wall can be considered straight as assumed implicitly in (9). This is however a mild constraint given that the characteristic scale of the network is horizon-size in the scaling regime, and we shall always assume that this condition is fulfilled.

seeded tunneling, and, as we shall see in Sec. V, it can nicely complement the KK method described above.

In order to evaluate the transition probability at finite temperature, we need to estimate the change in energy between the bounce configuration and the initial configuration. As a first approximation we can assume that the bounce respects an $O(3)$ symmetry and that it is described by a spherical bubble of radius R centered on the domain wall. The difference in energy between the bubble configuration and the false vacuum (corresponding to the unperturbed domain wall) is

$$E(R) = 4\pi R^2 \sigma_B - \frac{4}{3}\pi R^3 \Delta V - \pi R^2 \sigma_{DW}. \quad (37)$$

Here σ_B is the bubble tension and ΔV is the (positive) potential difference between the false and the true vacuum. The domain wall tension is

$$\sigma_{DW} = \frac{4}{3} \sqrt{\frac{\eta}{2}} v_s^3, \quad (38)$$

where v_s here denotes the temperature dependent vev of S . The first two terms in (37) are the usual surface term and volume term of a first order phase transition in homogeneous space [57, 65, 66]. Assuming that the presence of the domain wall does not affect significantly the shape and tension of the bubble, the tension σ_B can then be estimated with standard techniques developed for first order phase transitions. For the case of a model with two scalar fields we illustrate a procedure to derive it in Appendix A. The last term in (37) is due to the presence of the domain wall, and characterizes the energy difference between the initial configuration with an extended domain wall, and the bounce configuration where the domain wall has a hole of radius R . The critical radius for the bubble to be created thermally can be obtained by extremizing the energy with respect to R , finding $R_c = \frac{2}{\Delta V} (\sigma_B - \sigma_{DW}/4)$.

In Fig. 2 we display a representation of the energy of the nucleated bubble as a function of the radius R , both for the case without the domain wall corresponding to the homogeneous transition, and for the case with the domain walls. As it is clear also from Eq. (37), the presence of the domain wall makes the energy necessary to reach the critical radius smaller than in the case of the homogeneous transition. Note that this does not guarantee a priori that the seeded phase transition will dominate over the homogeneous one, since the nucleation condition is different, see Eqs. (3) and (6).

Given the expression for the energy (37), the rate for the thermal transition is $\propto \exp(-E(R_c)/T)$, and hence we can estimate the thermal bounce action as

$$\left(\frac{S_3}{T}\right)_{\text{TW}} \simeq \frac{16\pi (\sigma_B - \sigma_{DW}/4)^3}{3T\Delta V^2}, \quad (39)$$

where here the subscript indicates that we have considered an $O(3)$ spherical bubble geometry. Note that in the limit $\sigma_{DW} \rightarrow 0$ this expression reduces to the standard

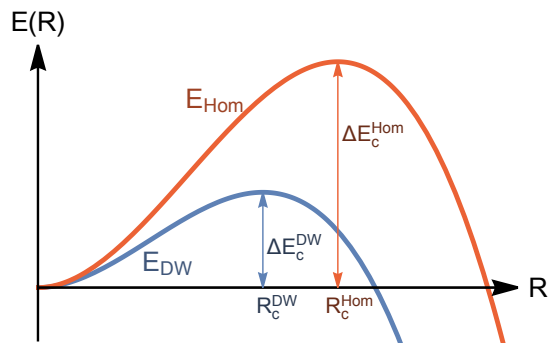


Figure 2. Energy of the bubble as a function of the radius. In red the standard case of homogeneous phase transition. In blue the case of a phase transition seeded by domain walls, where the bubble is encircling a disk of radius R on the domain wall. For the two cases, R_c^{Hom} and R_c^{DW} denote the critical bubble radius, while ΔE_c^{Hom} and ΔE_c^{DW} the energy necessary for the bubble to form. The inhomogeneous process results energetically favorable.

$O(3)$ bounce action for bubble nucleation for a homogeneous phase transition at finite temperature [57]. The net effect of the presence of the domain wall, in comparison with the homogeneous tunneling, is to reduce the bubble tension to an effective tension $\sigma_B - \sigma_{DW}/4$.

Let us now discuss how the previous estimate of the thin wall bounce action can be improved by taking into account that the symmetry of the bubble is actually not $O(3)$ but only $O(2)$. Indeed, when the domain wall tension is large and comparable to the bubble tension, the bubble of true vacuum has a lower energy if it gets flatter around the domain wall.

One may then consider different geometrical shapes for the bubble. A simple ansatz respecting a $O(2)$ symmetry is a spheroid centered on the domain wall with the two radii on the domain wall plane taken to be equal. In this case the energy difference between the bounce and the initial configuration is

$$E(R_1, R_2) = \Sigma(R_1, R_2)\sigma_B - \frac{4}{3}\pi R_1^2 R_2 \Delta V - \pi R_1^2 \sigma_{DW} \quad (40)$$

where R_1 is the size of the two radii in the plane of the domain wall, and R_2 is the radius perpendicular to the domain wall plane. $\Sigma(R_1, R_2)$ denotes the spheroid surface. Given the tensions and ΔV , this energy should be extremized numerically for R_1 and R_2 to find the critical radii R_1^c and R_2^c . The thermal bounce action is then estimated in this case as $(S_2/T)_{\text{TW}} \simeq E(R_1^c, R_2^c)/T$. Note that in principle, the bubble tension in (40) is also a function of the radii R_1 and R_2 , since it can change as a function of the curvature on the spheroid. In the following, we will instead approximate σ_B in (40) with the tension computed assuming $O(3)$ symmetry, which is an underestimate of the $O(2)$ tension.

Let us finally note that when the tension of the domain wall, σ_{DW} , becomes of the order of the bubble tension, σ_B , the critical radius in Fig. 2 goes to zero and so does

the bounce action, signalling that the phase transition is not first order. This behaviour actually corresponds to the same classical instability described in the previous sections, and it occurs at $\sigma_B \sim \sigma_{DW}/4$ and $\sigma_B \sim \sigma_{DW}/2$ for the $O(3)$ and $O(2)$ bounces, respectively. However, this typically happens at temperatures significantly lower than T_c where the thin wall approximation is not precise, and in the following we shall rely only on the condition discussed around Eq. (33) to identify this behaviour.

V. RESULTS

The Higgs–singlet model depends on three independent parameters (m_S, κ, η) according to the potential (7), where m_S is the singlet mass in the electroweak vacuum as given in (8). As mentioned in Sec. III, we will here focus on the region of parameter space where a two–step phase transition occurs, so that the domain walls formed in the first step can act as seeds for the second one.

The general outcome of our study is that the seeded vacuum decay is always found to be the fastest process compared to the homogeneous tunneling. In addition, regions of the parameter space where the fields would stay trapped if domain walls were neglected become now viable due to the seeded tunneling. An overview of our results is shown in Fig. 3 where we have performed a scan over the parameter space in terms of the portal coupling κ and the singlet quartic η , fixing the singlet mass to $m_S = 180$ GeV as a representative value.

The red–shaded regions in Fig. 3 are those where the homogeneous phase transition is expected to be first order. The corresponding tunneling rate is sufficiently fast until the red solid line is reached, below which bubbles fail to nucleate. When taking into account the presence of the domain walls, however, the phase transition is found to proceed always via seeded false vacuum decay in all the parameter space according to either of the mechanisms of Sec. II. In the dark red region this is due to the domain walls developing a classical instability above the critical temperature and then dissociating as soon as the temperature drops below T_c (see Sec. V A). In the light red region a classical instability is actually never developed, and the transition is completed via seeded bubble nucleation (see Sec. V B).

Within the blue region in Fig. 3, the phase transition can instead only proceed via seeded vacuum decay. The benchmark point indicated by the blue star in Fig. 3 will be studied in detail in Sec. V C where we estimate the nucleation temperature as well as the shape of the nucleated bubble. The seeded tunnelling stops being cosmologically fast below the purple line where the fields will remain trapped in the false vacuum.

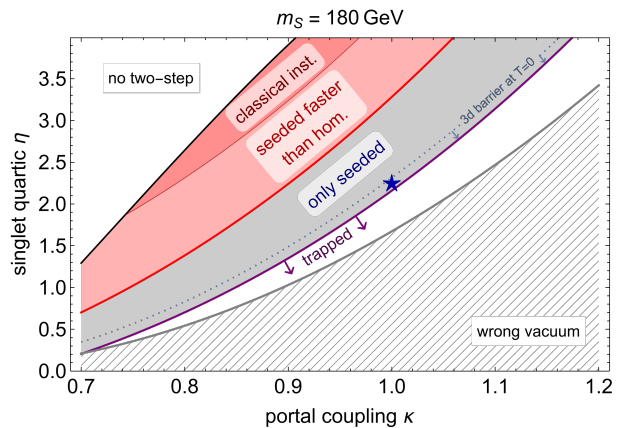


Figure 3. Scan in the (κ, η) parameter space for $m_S = 180$ GeV. The upper–left corner is excluded from our analysis as the phase transition does not follow the two–step path described in Sec. III. The bottom–right corner is also excluded as the electroweak minimum is not the true vacuum at zero temperature. The regions shaded in red indicate where a first order phase transition is expected due to homogeneous tunneling. Our analysis shows that the seeded false vacuum decay is instead the dominant process for completing the phase transition: in the dark red region this is because of a classical instability of the domain walls (rolling), whereas in the light red region this is due to the seeded nucleation being faster than the homogeneous one. In the blue region the homogeneous bubbles would actually fail to nucleate and the only relevant process there is seeded nucleation. Below the dotted blue line the barrier for the seeded tunneling persists also at zero temperature, and the fields may be trapped if the nucleation rate is too small. This is the case for the points below the purple line which are then not viable. The benchmark point close to the no–nucleation line indicated by the blue star will be discussed in detail in Sec. V C.

A. The rolling

We here discuss in more detail the case in which the domain walls become unstable already above the critical temperature. Let us assume that the first instability occurs at $T_r > T_c$ and corresponds to $\omega_0^2(T_r)$ turning negative. This signals that the linearized equation of motion for the 4d Higgs field in the domain wall background supports at least one solution in which perturbations grow exponentially in time. Since we are still above T_c , this will eventually result in a new (stable) domain wall configuration with a non–vanishing Higgs profile. When the temperature drops below T_c , these configuration will eventually dissociate completing the phase transition.

We shall first consider classical instability in a toy benchmark for which the new stable configuration above T_c can be obtained exactly, and later on discuss the relevance for the electroweak phase transition. This will allow us to validate our method based on the KK decomposition presented in Sec. IV by comparing it against these exact results.

Setting $\eta = 1$ and $m = 1$ (which is possible thanks to

field redefinitions and rescaling of the space time coordinates) the potential (7) will have a global minimum at $S = \pm 1$ for $\lambda > \mu^4$ allowing for the domain wall solution (9) (the temperature dependence is here left implicit). Focussing on the case where the remaining parameters are such that $\omega_0^2 < 0$, the new stable configuration can be obtained exactly for very special values of λ , see e.g. [61], namely $\lambda = \kappa(\kappa - 2\mu^2)/(2\kappa - 2\mu^2 - 1)$. The vacuum structure of this toy benchmark is then actually equivalent to have a Higgs instability above T_c , with the advantage that the stable profiles are known:

$$S(z) = \tanh(z/\delta), \quad (41)$$

$$h(z) = \sqrt{1/\kappa + 2\mu^2/\kappa - 2} \operatorname{sech}(z/\delta), \quad (42)$$

where $\delta = (\kappa - \mu^2)^{1/2}$.

We can now try to approximate this exact result in our 3d theory, where the problem of finding the stable configurations (41) and (42) is equivalent to searching for the minimum of the potential \tilde{V} . Discrete and scattering states will then take a vev in the new vacuum, thus modifying the overall profiles along z according to the superposition in (12).

In practice there are three ways to minimize the 3d potential: *i*) Include a (large enough) number of scattering states together with the discrete modes and minimize a multi field potential. This way is the most reliable but it may become unpractical for a large number of fields. *ii*) Include a (large enough) number of scattering states and integrate them out at tree level in favour of an effective potential for h_0 and s_0 only, according to the discussion in Sec. IV A. *iii*) Neglect the scattering states altogether and minimize the quartic potential for s_0 and h_0 in (26). This corresponds to the lowest level of accuracy.

We compare these different options in Fig. 4 for a representative choice of μ^2 and κ . The exact solutions (41) and (42) are shown by the blue lines. The results employing *i*) are shown in orange, where we have included KK states up to masses $\sim 10|\omega_0|$ for the two towers, and taking the size of the box to be $2L \simeq 50 m^{-1}$. The green line shows the solution integrating out KK states according to *ii*) up to masses $\sim 15|\omega_0|$ with $\mathcal{O}(1/m_{\text{KK}}^4)$ accuracy, using the same value for the size of the box. Finally, the red line is obtained by neglecting altogether the KK contribution to the potential according to *iii*), and is based on the terms given in (26).

As we can see, options *i*) and *ii*) provide a quantitative agreement with the exact result, and improve on the simplest approach *iii*). The location of the global minimum in terms of h_0 turns out to be $h_0 \simeq 1.7$, and the ratio in (29) evaluates to ~ 0.3 confirming the reliability of the expansion.

After having validated our 3d methods by reproducing these non-trivial results, let us now move to study more phenomenologically interesting benchmarks in the singlet-extended SM, where the unperturbed domain wall can develop an instability above T_c in some part of the parameter space.

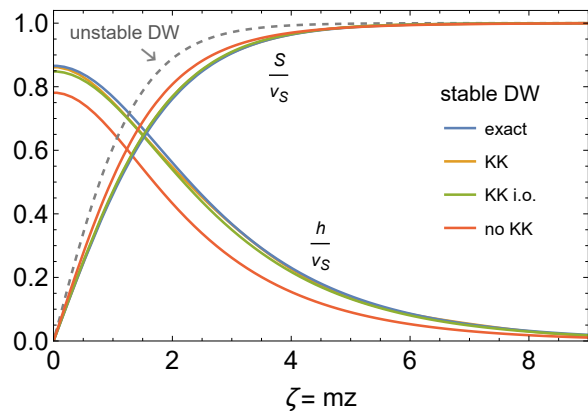


Figure 4. The new stable configuration approached by the system following an instability of the unperturbed domain wall above the critical temperature in a toy benchmark of the Higgs–singlet model. The h and S profiles are respectively even and odd for $z \rightarrow -z$. The dashed gray line shows the unperturbed domain wall which turns unstable when $\omega_0^2 < 0$. Blue lines show the exact profiles of the stable configuration. The remaining colorful lines approximate the exact solutions according to the 3d methods discussed in the text: *i*) minimizing the multi field potential (orange), *ii*) integrating out the KK fields at tree level and minimize the effective two-field potential for the discrete states (green), *iii*) neglect altogether the KK states and minimize the two-field potential for the discrete states (red). Once the minimum in terms of the 3d fields is found in the various approximation schemes, the overall profile along z can be reconstructed via (12). The model parameters were taken to be $m = 1$, $\eta = 1$, $\mu^2 = 5/12$ and $\kappa = 2/3$ (with these choices one also has $v_s = 1$).

We find that this is in fact the case in the region shaded in dark red in Fig. 3 for the choice $m_S = 180$ GeV, (whereas this is never realized in our other scan in Fig. 5 with $m_S = 250$ GeV). For these points we find that the rolling temperature T_r is only slightly above the critical temperature, so that a stable domain wall with a Higgs core may last only shortly. When the temperature drops below T_c , no global minimum is found in the region where the effective theory is valid, in agreement with the intuition that domain walls with a non-vanishing Higgs profile should start dissociating when the true vacuum is the one with $S = 0$.

The seeded vacuum decay in this case may resemble a very weakly first-order electroweak phase transition occurring at T_c , with the notable difference that the process is not controlled by the bubble nucleation rate, but rather by the number of domain walls per hubble patch and their velocity [7]. This means that the time for completing the phase transition may differ significantly when compared to this first-order analogue. Possible phenomenological implications are discussed in more detail in Sec. VI.

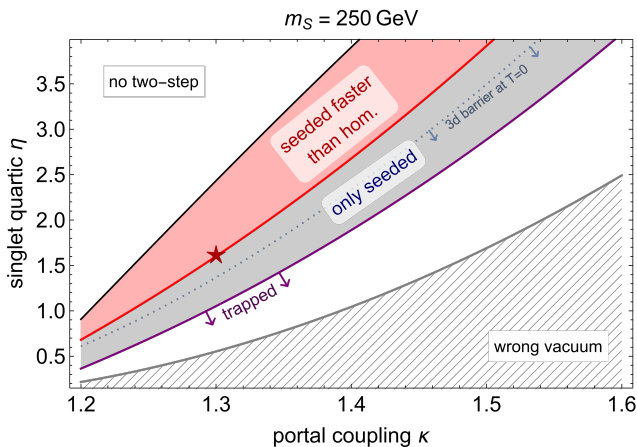


Figure 5. Scan in the (κ, η) parameter space for $m_S = 250$ GeV. The meaning of the various labels is the same as in Fig. 3. In the light red region a two-step first order phase transition is expected due to homogeneous tunneling. Seeded nucleation is however faster and it will be the leading mechanism for completing the phase transition. In the blue region homogeneous bubbles fail to nucleate but the transition still completes due to the seeded vacuum decay. Below the purple line even the seeded nucleation becomes cosmologically slow and the fields are trapped in the false vacuum. The point marked by the red star is studied in detail in Fig. 6.

B. The tunneling

Let us now move to investigate the other possibility in which the mass of the discrete Higgs mode $\omega_0^2(T)$ is positive for a range of temperatures below T_c , implying that the seeded phase transition will proceed via bubbles nucleated inside the domain walls.

As mentioned at the beginning of this section, this process is the relevant one in the parameter space shaded in light red in Fig. 3 with $m_S = 180$ GeV. The same behaviour persists also when changing the mass of the singlet scalar to $m_S = 250$ GeV, as shown in Fig. 5 (with the only qualitative difference that the region of classical instability is no longer found).

In order to assess whether the phase transition will be completed via homogeneous or seeded tunneling, we have compared the homogeneous action S_3/T with the inhomogeneous action S_2/T , taking into account the different nucleation conditions derived in Sec. II.

The bounce action S_3/T can be evaluated as a function of the temperature with the help of `CosmoTransitions` and `FindBounce` from the temperature-dependent 4d potential. As mentioned in Sec. IV, a full-fledged implementation of the thermal corrections is challenging for the formalism based on dimensional reduction. In order to make a consistent comparison we shall then use the high temperature approximation also for S_3/T .

The action S_2/T can be computed in the 3d theory following three levels of approximations similarly to what discussed in the previous subsection. The difference here

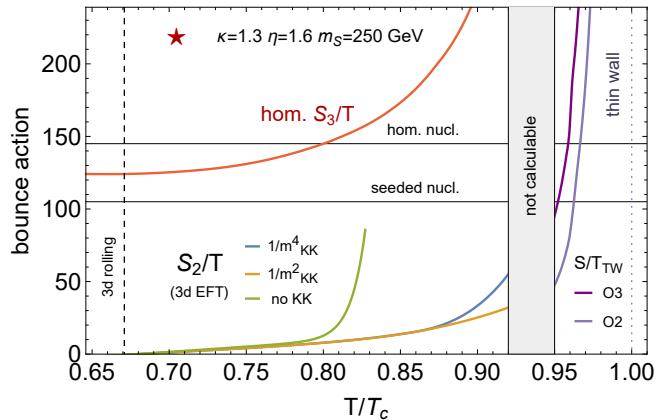


Figure 6. Benchmark point for $m_S = 250$ GeV with $\kappa = 1.3$ and $\eta = 1.6$. The gray horizontal lines indicate the thresholds for a cosmologically fast tunneling at the electroweak scale for a homogeneous phase transition and for a transition seeded by domain walls, as discussed in Sec. II. The dashed vertical line indicates the temperature at which the (thermal) barrier for the seeded tunneling vanishes so that the corresponding bounce action approaches zero. The red line refers to the S_3/T action for the homogeneous tunneling. The inhomogeneous action S_2/T is shown according to the various approximations discussed in the text, namely neglecting the continuum KK states (green), in the effective theory at $\mathcal{O}(1/m_{\text{KK}}^2)$ (orange) and $\mathcal{O}(1/m_{\text{KK}}^4)$ (blue) accuracy, and in the thin wall approximation, which is reliable close to the critical temperature, with a $O(3)$ (purple) and $O(2)$ (light purple) ansatz for the bubble. By this latter method we estimate the nucleation temperature to be $\sim 0.96 T_c$ in this benchmark. The gray-shaded area corresponds to the temperature range in which none of the various methods implemented here can be applied reliably.

is that the option *i*) that keeps the KK states in the theory becomes quickly unpractical as this would require to solve a multi-field bounce. For this reason, we will only study the two-field problem for the discrete modes h_0 and s_0 with different level of accuracy, namely in the effective theory where the continuum KK states are integrated out at $\mathcal{O}(1/m_{\text{KK}}^4)$ and $\mathcal{O}(1/m_{\text{KK}}^2)$, and neglecting the KK states altogether. Once the effective potential is obtained with these different approximations, we can find the bounce solution with the help of `CosmoTransitions` since the $O(2)$ bounce requires to set $d = 2$ for the space-time dimension.

A comparison between the various tunneling rates for the benchmark indicated by the red star in Fig. 5 with $m_S = 250$ GeV, $\kappa = 1.3$ and $\eta = 1.6$, is shown in Fig. 6. For this benchmark the critical temperature is $T_c \simeq 110$ GeV, whereas the spontaneous Z_2 breaking happens at $T_d \simeq 140$ GeV. The 4d theory is such that the barrier between the false $(0, v_s)$ and true $(v, 0)$ vacuum is non-vanishing also at zero temperature. On the other hand, the h_0 mass in the 3d theory turns negative at the would-be rolling temperature $T_r \simeq 0.67 T_c$, meaning that the

barrier for the seeded tunneling is only thermal.

The homogeneous bounce action is plotted in red and the nucleation condition is satisfied at $T \sim 0.8T_c$. The action S_2/T for the seeded tunneling is shown according to the various approximations at the order $\mathcal{O}(1/m_{\text{KK}}^4)$ (blue), $\mathcal{O}(1/m_{\text{KK}}^2)$ (orange), and neglecting the continuum states (green). At low temperatures close to the rolling at T_r , the barrier is small and the release point is very close to the origin. The effective operators arising from the exchange of the KK states are thus suppressed and all the approximation schemes give the same result. At higher temperatures the effect of the continuum states is more and more important, and around $T/T_c \sim 0.82$ it becomes crucial in making the origin $(0,0)_{3d}$ metastable. For this reason the prediction obtained considering only the discrete states starts departing from the other two.

The effective theories at $\mathcal{O}(1/m_{\text{KK}}^2)$ and $\mathcal{O}(1/m_{\text{KK}}^4)$ still agree with each other for $T \lesssim 0.9T_c$. For higher temperatures the release point starts to leave the region of validity, with (28) being $\gtrsim \mathcal{O}(1)$, and calculability is lost. This corresponds to the gray-shaded region in Fig. 6. In fact, very close to T_c the energy difference between the false and true vacuum is small. This means that a larger bubble is needed for the energy gain to compensate its tension. This bubble will then become more and more spherical, thus probing more and more the direction orthogonal to the domain wall. From the point of view of our 3d theory, this requires a large number of KK continuum states to be excited, thus explaining the loss of validity of the effective theory.

However, in this very limit the bubble wall becomes thin, so that we can apply the approximation discussed in Sec. IV B. The prediction according to the $O(3)$ and $O(2)$ bounce actions in the thin wall limit are shown in Fig. 6 by the purple and light purple line, respectively, until $T = 0.95T_c$, below which the thin wall approximation becomes less accurate. This information can nonetheless be used to estimate the nucleation temperature to be around $T \sim 0.96T_c$ in this benchmark, and to complement the effective theory calculation of S_2/T in the region close to the critical temperature. For illustration, in Appendix B we employ the thin wall approximation to estimate the nucleation temperature also for other points in the parameter space explored in Fig. 5.

We can then summarize our findings as follows. First of all, it is clear that in this benchmark point the seeded tunnelling is faster than the homogeneous one, since at the time of the would-be homogeneous nucleation the seeded bounce action is well below its nucleation condition. The light red regions in Fig. 3 and Fig. 5 are in fact identified in this way.

Secondly, we have encountered a rather generic feature of the 3d effective theory, namely the fact that it works the best at lower temperatures where the bubble is thick, and that it will necessarily break down close to the critical temperature. This shows an interesting complementarity with the thin wall approximation, which is instead most reliable in the opposite regime close to T_c .

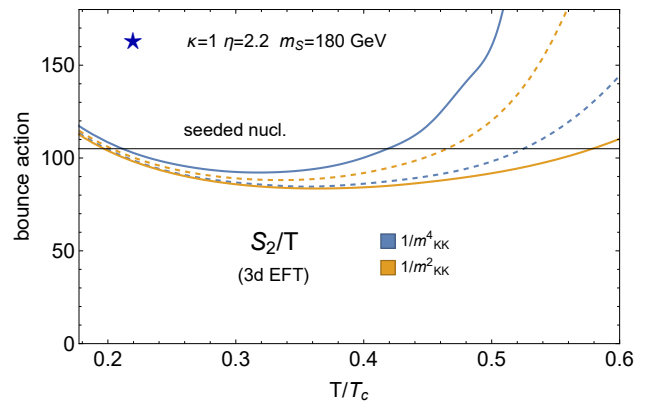


Figure 7. Benchmark point for $m_s = 180$ GeV with $\kappa = 1$ and $\eta = 2.2$. The horizontal gray line indicates the nucleation condition for a phase transition catalyzed by the domain walls. The solid lines show the bounce action S_2/T as obtained within the effective 3d theory at $\mathcal{O}(1/m_{\text{KK}}^4)$ (blue) and $\mathcal{O}(1/m_{\text{KK}}^2)$ (orange). Dashed lines are shown as a further estimate of the theoretical uncertainty as explained in the text. The approximation scheme in which the continuum states are neglected is unable to identify the metastability of the false vacuum and no prediction for the tunneling can be obtained.

In general, a gap of calculability is expected for intermediate temperatures, as indicated by the gray zone in Fig. 6.

C. The bubble

As discussed in the previous subsection, the closer the seeded nucleation is to the critical temperature the more we can expect the bubbles to approach a spherical symmetry. Away from this limit, instead, the presence of the catalyzing domain wall will generally favor a spheroidal shape in which the size of the critical bubble along the domain wall plane is bigger than the one in the orthogonal z direction.

Let us here investigate the properties of the seeded bubbles in detail within the 3d formalism for the benchmark point indicated by the blue star in Fig. 3 with $m_s = 180$ GeV, $\kappa = 1$ and $\eta = 2.2$. The critical temperature is $T_c \simeq 60$ GeV, whereas $T_d \simeq 180$ GeV. In this region of parameter space the homogeneous nucleation is very slow and the transition can be completed only via seeded tunneling. This benchmark is also rather close to the no-nucleation condition, so that we can expect the transition to take place significantly below the critical temperature, where the thin wall approximation can be hardly applied. In addition, the 3d barrier here persists also at $T = 0$ so that the bounce action S_2/T will asymptotically grow at low temperatures.

Our results for S_2/T are presented in Fig. 7. In the simplest approximation that neglects the continuum KK states, the metastability of the 3d vacuum $(0,0)_{3d}$ is not

captured at all, and thus no prediction for the tunneling can be obtained (unlike for the benchmark point shown in Fig. 6, where the vanishing of the barrier at the rolling temperature ensures a range of validity for this approach).

The solid lines in Fig. 7 are obtained according to the effective 3d potential at $\mathcal{O}(1/m_{\text{KK}}^4)$ (blue) and $\mathcal{O}(1/m_{\text{KK}}^2)$ (orange). The dashed lines are similarly based on integrating out the KK states with the corresponding accuracy. The actual effective potential for h_0 and s_0 is however re-evaluated by substituting the profiles of the KK states obtained as a function of h_0, s_0 back in the 4d potential. The numerical integration over z then gives an effective 3d potential that contains higher-order terms. The discrepancy between the dashed and solid lines can then be used as a further estimate of the theoretical uncertainty.

As we can see from Fig. 7, all the different levels of approximation agree at lower temperatures as the release point is there closer to the origin. This is already enough to conclude that the phase transition will certainly be completed as there is a range of temperatures for which S_2/T is below the nucleation condition with small uncertainty. Points belonging to the blue regions in the scan plots of Fig. 3 and Fig. 5 are in fact conservatively determined in this way.

At higher temperatures, the release point moves further away from the origin and the theoretical uncertainty increases. We can nonetheless estimate the nucleation to be at $T \sim 0.5 T_c$ according to the dashed blue line, and look at the bounce solution at this temperature to illustrate the general shape of the seeded bubbles.

The Higgs and singlet bounce profiles at the estimated nucleation temperature are shown in Fig. 8 as contour plots in the (ρ, ζ) plane, where $\rho = mr$ is the polar coordinate in the domain wall plane rescaled by the inverse of the domain wall width, and similarly for $\zeta = mz$ along the orthogonal direction. The Higgs profile is shown by three contour levels where it is 0.8 (solid), 0.6 (dashed) and 0.4 (dotted) times the value that it takes at the center of the bubble ($r = 0, z = 0$), denoted by $v_r \simeq 200$ GeV. The singlet profile is normalized to its vev in the false vacuum, $v_s \simeq 110$ GeV, and is shown as a density plot according to the orange color code.

Far from the bubble for $\rho \rightarrow \infty$, the unperturbed, straight, domain wall interpolating between $S = \pm v_s$ is recovered, and the Higgs field takes a negligible vev. Similarly for $z \rightarrow \pm\infty$ the system approaches the false vacuum $(0, \pm v_s)$, in agreement with the boundary conditions in Sec. II.

Around $\rho, \zeta = 0$, we can see that a bubble of true vacuum has been nucleated with the original domain wall profile rearranging to host a non-vanishing Higgs vev. We also note that the shape of the bubble resembles more the one of a disk, or of a spheroid, rather than a sphere, with the size in the domain wall plane being ~ 4 times larger than the one along the orthogonal direction.

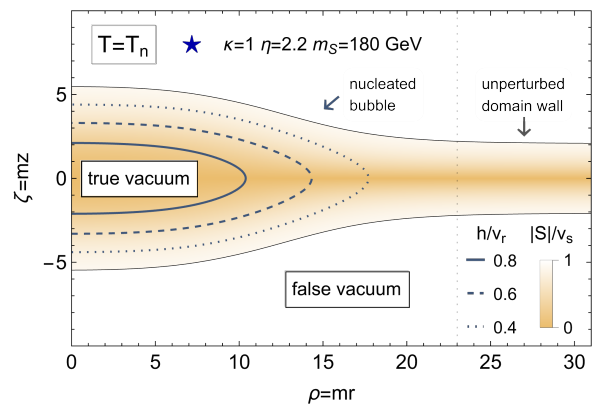


Figure 8. The shape of a bubble of true vacuum at the nucleation temperature in the benchmark point with $m_S = 180$ GeV, $\kappa = 1$ and $\eta = 2.2$ as a function of the natural variables $\rho = mr$ and $\zeta = mz$. The Higgs field is shown as contour levels where it takes values 0.8 (solid), 0.6 (dashed) and 0.4 (dotted) times the vev at the center of the bubble, $v_r \simeq 200$ GeV at $(r = 0, z = 0)$. The singlet field normalized to $v_s \simeq 110$ GeV is shown according to the color code in orange. The unperturbed domain wall profile at $\rho \rightarrow \infty$ is modified to host a non vanishing Higgs vev at $\rho = 0$. For $\zeta \rightarrow \pm\infty$ the false vacuum ($h = 0, S = \pm v_s$) is approached everywhere.

VI. DISCUSSION

Our results in Sec. V show that domain walls can act as local impurities at the time of electroweak symmetry breaking, and can thus have a strong impact on the dynamics of the phase transition. Interestingly, all the ingredients for this to occur are already present in the minimal extension of the SM including a Z_2 -odd real scalar singlet undergoing a two-step phase transition. The tunneling process catalyzed by the domain walls is studied with a new method based on dimensional reduction, by which the seeded phase transition is reduced to a standard homogeneous problem in 3d, and in a complementary way by employing the thin wall approximation. Our conclusion is that in the parameter space under consideration the vacuum decay seeded by domain walls is always faster than the homogeneous tunneling, and it ultimately determines the phenomenological properties of the phase transition. In addition, new regions of parameter space where the fields would be trapped in the false vacuum become now viable as a result of the inhomogeneous tunneling.

We shall now discuss the phenomenological implications of a catalyzed electroweak phase transition.

First of all, the gravitational wave signal in this scenario will be mainly controlled by the parameter ξ counting the number of defects per Hubble volume [7]. This in fact determines the duration of the phase transition by setting the initial average distance between the domain walls. In the case of rolling, the walls will start disso-

ciating as a whole with velocity v around T_c , and will then collide with an inverse time scale $\sim v\xi(T_c)H$. If instead the transition proceeds by inhomogeneous tunneling, bubbles will be nucleated on the domain walls with a standard rate $\sim 100H$ setting the time scale for the collisions inside the domain walls. The collision with bubbles from the nearby walls will on the other hand depend on the average distance, thus giving an inverse time scale $\sim v\xi(T_n)H$. Characteristic features may then appear in the gravitational wave spectrum associated to these two types of collisions.

The amplitude of the gravitational wave signal from a catalyzed phase transition can then be significantly larger than the one from its homogeneous counterpart provided that $\xi < 100$, as this effectively corresponds to take a naturally smaller value for the inverse duration of the phase transition. Two-step phase transitions in which there is a larger gap in temperature between the steps are more promising in this regard, as domain walls will have more time to reach the scaling regime where $\xi \sim \mathcal{O}(1)$. In addition, the sizeable violation of spherical symmetry of the seeded bubbles can contribute to increase the production of gravitational waves. A quantitative analysis of these different effects is left for future work.

Let us now comment on how electroweak baryogenesis may be realized in this scenario in connection with a possible origin of the Z_2 symmetry. The singlet and the Higgs scalars may in fact arise as pseudo Nambu–Goldstone bosons in the next-to-minimal composite Higgs model [67] based on the $SU(4)/Sp(4)$ coset. The Z_2 symmetry comes then from the automorphisms of this coset and can be identified with \mathcal{CP} in the scalar sector, with the Higgs and the singlet being even and odd, respectively. Since a vacuum expectation value for S breaks \mathcal{CP} spontaneously, the model can lead to successful electroweak baryogenesis during the second step of the phase transition. However, if the two possible configurations $\langle S \rangle = \pm v_s$ are equally probable, any asymmetry produced via this mechanism will eventually average out when combining the contributions of the two different domains. This issue was circumvented in Refs. [54, 60] by adding a small explicit breaking of \mathcal{CP} so that domain walls will collapse before the electroweak phase transition, leaving the Universe with a single homogeneous value of v_s when baryogenesis takes place. Alternatively, the Z_2 symmetry may never be restored at high temperatures eliminating altogether the formation of the different domains [68]. However we remark that the presence of a small bias induced by Planck-suppressed operators (as discussed in Sec. III) could prevent the cancellation of the baryon asymmetry by favoring a slightly larger volume corresponding to one minimum over the other, as also noted in Ref. [54], without necessarily collapsing the domain walls at the time of the electroweak phase transition.

Let us conclude this section by noticing that defects, and in particular domain walls, can form and act as impurities also in models with a richer symmetry breaking

pattern than the one studied in this paper. This may occur for instance in extensions of the SM with new electroweak scalars [69–72], but it can also be relevant for symmetry breaking chains happening at higher energies in scenarios where the SM gauge group is embedded in a larger group [73–76]. We expect that the strategy developed here may be similarly applied to these scenarios as well, possibly involving other types of defects such as for instance in the case of cosmic strings.

ACKNOWLEDGEMENTS

We are grateful to Riccardo Argurio and Diego Redigolo for useful discussions and comments on the draft. We also thank Luigi Tizzano and Iason Baldes for useful discussions.

SB and AM are supported by the Strategic Research Program High-Energy Physics and the Research Council of the Vrije Universiteit Brussel, and by the “Excellence of Science - EOS” - be.h project n.30820817.

Appendix A: Bubble tension in the thin wall approximation

In this Appendix we discuss how we can estimate the tension of the bubble in the thin wall limit for a multi-field potential. The tension in the thin wall approximation is the one-dimensional bounce action evaluated across the bubble wall [57, 65, 66]

$$S_1 = \int_{R-\delta R}^{R+\delta R} \sum_i \frac{1}{2} \left(\frac{d\phi_i}{dr} \right)^2 + V(\phi_i) dr, \quad (\text{A1})$$

where we will normalize $V(\phi_i^f) = 0$ for simplicity. Using the equation of motion in the thin wall approximation, one can simplify this expression and get

$$S_1 = \int_{R-\delta R}^{R+\delta R} 2V(\phi_i) dr. \quad (\text{A2})$$

Since the expressions for the bounce profiles ϕ_i are not known, it is useful to make a change of variables in the integral, moving from the radius to the fields themselves as done in the standard one-field case. In multi-field potentials, this is complicated by the fact that we do not know the path in field space that minimizes the tension. We shall here consider as optimal path the one that minimizes the scalar potential $V(\phi_i)$. Specializing to the two field case (having in mind the application to the Higgs-singlet model of the main text), we can parametrize this path by using ϕ_1 and defining a function

$$\phi_2(\phi_1) \quad \text{with} \quad \phi_2(\phi_1^f) = \phi_2^f \quad \phi_2(\phi_1^t) = \phi_2^t \quad (\text{A3})$$

that follows the path that minimizes the scalar potential. The function $\phi_2(\phi_1)$ can be easily found numerically. We

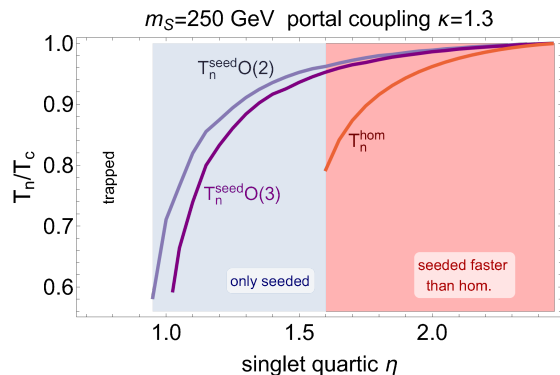


Figure 9. Nucleation temperature normalized to the critical temperature in the slice of parameter space obtained by fixing $m_S = 250$ GeV and $\kappa = 1.3$. The red line shows the nucleation temperature of the homogeneous phase transition, T_n^{hom} , computed numerically with `FindBounce`. The inhomogeneous nucleation temperature in the thin wall approximation is shown according to the $O(3)$ and $O(2)$ ansatz by the purple and light purple line, respectively. The color shading of the regions has the same meaning as in Fig. 5.

can then make the change of variable from r to ϕ_1 and find the Jacobian of the transformation by using again the equation of motions in the thin wall approximation. We then obtain

$$S_1 = \int_{\phi_1^*}^{\phi_1^f} \sqrt{1 + \left(\frac{d\phi_2}{d\phi_1}\right)^2} \sqrt{2V(\phi_1, \phi_2(\phi_1))} d\phi_1. \quad (\text{A4})$$

In order to minimize the tension, the lower extremum of the integral is defined as the closest point to ϕ_1^f along the path such that $V(\phi_1^*, \phi_2(\phi_1^*)) = V(\phi_1^f, \phi_2^f)$. As expected, this expression reduces to the standard thin wall tension for one-field if ϕ_2 is actually a constant along the path.

Appendix B: Estimate of the nucleation temperature

In this Appendix we push the thin wall approximation to its limit of validity and estimate the nucleation temperature moving more and more away from T_c . We consider a vertical slice of the parameter space explored in Fig. 5 by fixing $\kappa = 1.3$ while varying η . For each value of η we compute the $O(3)$ and $O(2)$ thin wall bounce action as described in Section IV B, and we derive the corresponding nucleation temperature by the condition (6). Our results are shown in Fig. 9, where we have also included the homogeneous nucleation temperature T_n^{hom} evaluated with `FindBounce` for comparison.

As we can see, the $O(2)$ and $O(3)$ approximations give similar results close to T_c , with the $O(2)$ ansatz providing in general a higher nucleation temperature (or equivalently a smaller action). The behaviour shown in Fig. 9 agrees with the picture that the seeded phase transition on the domain walls anticipates the would-be homogeneous nucleation, as $T_n^{\text{seed}} > T_n^{\text{hom}}$ for all the relevant values of η .

-
- [1] E. Barausse et al., *Prospects for Fundamental Physics with LISA*, *Gen. Rel. Grav.* **52** (2020), no. 8 81, [[arXiv:2001.09793](#)].
- [2] R. Caldwell et al., *Detection of Early-Universe Gravitational Wave Signatures and Fundamental Physics*, in *2022 Snowmass Summer Study*, 3, 2022, [arXiv:2203.07972](#).
- [3] P. J. Steinhardt, *Monopole and Vortex Dissociation and Decay of the False Vacuum*, *Nucl. Phys. B* **190** (1981) 583–616.
- [4] P. J. Steinhardt, *Monopole Dissociation in the Early Universe*, *Phys. Rev. D* **24** (1981) 842.
- [5] L. G. Jensen and P. J. Steinhardt, *DISSOCIATION OF ABRIKOSOV-NIELESEN-OLESEN VORTICES*, *Phys. Rev. B* **27** (1983) 5549.
- [6] Y. Hosotani, *Impurities in the Early Universe*, *Phys. Rev. D* **27** (1983) 789.
- [7] E. Witten, *Cosmic separation of phases*, *Phys. Rev. D* **30** (Jul, 1984) 272–285.
- [8] W. A. Hiscock, *CAN BLACK HOLES NUCLEATE VACUUM PHASE TRANSITIONS?*, *Phys. Rev. D* **35** (1987) 1161–1170.
- [9] D. R. Green, E. Silverstein, and D. Starr, *Attractor explosions and catalyzed vacuum decay*, *Phys. Rev. D* **74** (2006) 024004, [[hep-th/0605047](#)].
- [10] R. Gregory, I. G. Moss, and B. Withers, *Black holes as bubble nucleation sites*, *JHEP* **03** (2014) 081, [[arXiv:1401.0017](#)].
- [11] P. Burda, R. Gregory, and I. Moss, *Vacuum metastability with black holes*, *JHEP* **08** (2015) 114, [[arXiv:1503.07331](#)].
- [12] K. Mukaida and M. Yamada, *False Vacuum Decay Catalyzed by Black Holes*, *Phys. Rev. D* **96** (2017), no. 10 103514, [[arXiv:1706.04523](#)].
- [13] B. K. El-Menoufi, S. J. Huber, and J. P. Manuel, *Black holes seeding cosmological phase transitions*, [arXiv:2006.16275](#).
- [14] N. Oshita, M. Yamada, and M. Yamaguchi, *Compact objects as the catalysts for vacuum decays*, *Phys. Lett. B* **791** (2019) 149–155, [[arXiv:1808.01382](#)].
- [15] R. Balkin, J. Serra, K. Springmann, S. Stelzl, and A. Weiler, *Density Induced Vacuum Instability*, [arXiv:2105.13354](#).
- [16] U. A. Yajnik, *PHASE TRANSITION INDUCED BY COSMIC STRINGS*, *Phys. Rev. D* **34** (1986) 1237–1240.
- [17] U. A. Yajnik and T. Padmanabhan, *ANALYTICAL APPROACH TO STRING INDUCED PHASE TRANSITION*, *Phys. Rev. D* **35** (1987) 3100.
- [18] J. Preskill and A. Vilenkin, *Decay of metastable topological defects*, *Phys. Rev. D* **47** (1993) 2324–2342, [[hep-ph/9209210](#)].
- [19] I. Dasgupta, *Vacuum tunneling by cosmic strings*, *Nucl. Phys. B* **506** (1997) 421–435, [[hep-th/9702041](#)].

- [20] B. Kumar and U. A. Yajnik, *On stability of false vacuum in supersymmetric theories with cosmic strings*, *Phys. Rev. D* **79** (2009) 065001, [arXiv:0807.3254].
- [21] B.-H. Lee, W. Lee, R. MacKenzie, M. B. Paranjape, U. A. Yajnik, and D.-h. Yeom, *Battle of the bulge: Decay of the thin, false cosmic string*, *Phys. Rev. D* **88** (2013), no. 10 105008, [arXiv:1310.3005].
- [22] B. Kumar and U. Yajnik, *Graceful exit via monopoles in a theory with O’Raifeartaigh type supersymmetry breaking*, *Nucl. Phys. B* **831** (2010) 162–177, [arXiv:0908.3949].
- [23] B. Kumar, M. B. Paranjape, and U. A. Yajnik, *Fate of the false monopoles: Induced vacuum decay*, *Phys. Rev. D* **82** (2010) 025022, [arXiv:1006.0693].
- [24] B.-H. Lee, W. Lee, R. MacKenzie, M. B. Paranjape, U. A. Yajnik, and D.-h. Yeom, *Tunneling decay of false vortices*, *Phys. Rev. D* **88** (2013) 085031, [arXiv:1308.3501].
- [25] I. Koga, S. Kuroyanagi, and Y. Ookouchi, *Instability of Higgs Vacuum via String Cloud*, *Phys. Lett. B* **800** (2020) 135093, [arXiv:1910.02435].
- [26] D. I. Dunskey, A. Ghoshal, H. Murayama, Y. Sakakihara, and G. White, *Gravitational Wave Astronomy*, arXiv:2111.08750.
- [27] P. Agrawal and M. Nee, *The Boring Monopole*, arXiv:2202.11102.
- [28] G. Isidori, G. Ridolfi, and A. Strumia, *On the metastability of the standard model vacuum*, *Nucl. Phys. B* **609** (2001) 387–409, [hep-ph/0104016].
- [29] G. Degrossi, S. Di Vita, J. Elias-Miro, J. R. Espinosa, G. F. Giudice, G. Isidori, and A. Strumia, *Higgs mass and vacuum stability in the Standard Model at NNLO*, *JHEP* **08** (2012) 098, [arXiv:1205.6497].
- [30] D. Buttazzo, G. Degrossi, P. P. Giardino, G. F. Giudice, F. Sala, A. Salvio, and A. Strumia, *Investigating the near-criticality of the Higgs boson*, *JHEP* **12** (2013) 089, [arXiv:1307.3536].
- [31] Y. B. Zeldovich, I. Y. Kobzarev, and L. B. Okun, *Cosmological Consequences of the Spontaneous Breakdown of Discrete Symmetry*, *Zh. Eksp. Teor. Fiz.* **67** (1974) 3–11.
- [32] T. W. B. Kibble, *Topology of Cosmic Domains and Strings*, *J. Phys. A* **9** (1976) 1387–1398.
- [33] J. McDonald, *Gauge singlet scalars as cold dark matter*, *Phys. Rev. D* **50** (1994) 3637–3649, [hep-ph/0702143].
- [34] C. P. Burgess, M. Pospelov, and T. ter Veldhuis, *The Minimal model of nonbaryonic dark matter: A Singlet scalar*, *Nucl. Phys. B* **619** (2001) 709–728, [hep-ph/0011335].
- [35] J. R. Espinosa and M. Quiros, *Novel Effects in Electroweak Breaking from a Hidden Sector*, *Phys. Rev. D* **76** (2007) 076004, [hep-ph/0701145].
- [36] S. Profumo, M. J. Ramsey-Musolf, and G. Shaughnessy, *Singlet Higgs phenomenology and the electroweak phase transition*, *JHEP* **08** (2007) 010, [arXiv:0705.2425].
- [37] V. Barger, P. Langacker, M. McCaskey, M. J. Ramsey-Musolf, and G. Shaughnessy, *LHC Phenomenology of an Extended Standard Model with a Real Scalar Singlet*, *Phys. Rev. D* **77** (2008) 035005, [arXiv:0706.4311].
- [38] J. R. Espinosa, T. Konstandin, J. M. No, and M. Quiros, *Some Cosmological Implications of Hidden Sectors*, *Phys. Rev. D* **78** (2008) 123528, [arXiv:0809.3215].
- [39] J. R. Espinosa, T. Konstandin, and F. Riva, *Strong Electroweak Phase Transitions in the Standard Model with a Singlet*, *Nucl. Phys. B* **854** (2012) 592–630, [arXiv:1107.5441].
- [40] J. M. Cline and K. Kainulainen, *Electroweak baryogenesis and dark matter from a singlet Higgs*, *JCAP* **01** (2013) 012, [arXiv:1210.4196].
- [41] S. Profumo, M. J. Ramsey-Musolf, C. L. Wainwright, and P. Winslow, *Singlet-catalyzed electroweak phase transitions and precision Higgs boson studies*, *Phys. Rev. D* **91** (2015), no. 3 035018, [arXiv:1407.5342].
- [42] L. Feng, S. Profumo, and L. Ubaldi, *Closing in on singlet scalar dark matter: LUX, invisible Higgs decays and gamma-ray lines*, *JHEP* **03** (2015) 045, [arXiv:1412.1105].
- [43] D. Curtin, P. Meade, and C.-T. Yu, *Testing Electroweak Baryogenesis with Future Colliders*, *JHEP* **11** (2014) 127, [arXiv:1409.0005].
- [44] N. Craig, H. K. Lou, M. McCullough, and A. Thalappilil, *The Higgs Portal Above Threshold*, *JHEP* **02** (2016) 127, [arXiv:1412.0258].
- [45] P. Huang, A. J. Long, and L.-T. Wang, *Probing the Electroweak Phase Transition with Higgs Factories and Gravitational Waves*, *Phys. Rev. D* **94** (2016), no. 7 075008, [arXiv:1608.06619].
- [46] V. Vaskonen, *Electroweak baryogenesis and gravitational waves from a real scalar singlet*, *Phys. Rev. D* **95** (2017), no. 12 123515, [arXiv:1611.02073].
- [47] D. Curtin, P. Meade, and H. Ramani, *Thermal Resummation and Phase Transitions*, *Eur. Phys. J. C* **78** (2018), no. 9 787, [arXiv:1612.00466].
- [48] G. Kurup and M. Perelstein, *Dynamics of Electroweak Phase Transition In Singlet-Scalar Extension of the Standard Model*, *Phys. Rev. D* **96** (2017), no. 1 015036, [arXiv:1704.03381].
- [49] D. Buttazzo, D. Redigolo, F. Sala, and A. Tesi, *Fusing Vectors into Scalars at High Energy Lepton Colliders*, *JHEP* **11** (2018) 144, [arXiv:1807.04743].
- [50] C. Caprini et al., *Detecting gravitational waves from cosmological phase transitions with LISA: an update*, *JCAP* **03** (2020) 024, [arXiv:1910.13125].
- [51] T. Alanne, T. Hugle, M. Platscher, and K. Schmitz, *A fresh look at the gravitational-wave signal from cosmological phase transitions*, *JHEP* **03** (2020) 004, [arXiv:1909.11356].
- [52] A. Costantini, F. De Lillo, F. Maltoni, L. Mantani, O. Mattelaer, R. Ruiz, and X. Zhao, *Vector boson fusion at multi-TeV muon colliders*, *JHEP* **09** (2020) 080, [arXiv:2005.10289].
- [53] H. Al Ali et al., *The Muon Smasher’s Guide*, arXiv:2103.14043.
- [54] J. R. Espinosa, B. Gripaios, T. Konstandin, and F. Riva, *Electroweak Baryogenesis in Non-minimal Composite Higgs Models*, *JCAP* **01** (2012) 012, [arXiv:1110.2876].
- [55] S. Coleman, *Fate of the false vacuum: Semiclassical theory*, *Phys. Rev. D* **15** (May, 1977) 2929–2936.
- [56] A. D. Linde, *Fate of the False Vacuum at Finite Temperature: Theory and Applications*, *Phys. Lett. B* **100** (1981) 37–40.
- [57] A. D. Linde, *Decay of the False Vacuum at Finite Temperature*, *Nucl. Phys. B* **216** (1983) 421. [Erratum: Nucl.Phys.B 223, 544 (1983)].
- [58] J. Ellis, M. Lewicki, and J. M. No, *On the Maximal*

- Strength of a First-Order Electroweak Phase Transition and its Gravitational Wave Signal*, *JCAP* **04** (2019) 003, [[arXiv:1809.08242](#)].
- [59] A. Vilenkin and E. P. S. Shellard, *Cosmic Strings and Other Topological Defects*. Cambridge University Press, 7, 2000.
- [60] J. McDonald, *Cosmological domain wall evolution and spontaneous CP violation from a gauge singlet scalar sector*, *Phys. Lett. B* **357** (1995) 19–28.
- [61] R. Rajaraman, *SOLITONS AND INSTANTONS. AN INTRODUCTION TO SOLITONS AND INSTANTONS IN QUANTUM FIELD THEORY*. 1982.
- [62] E. Witten, *Superconducting Strings*, *Nucl. Phys. B* **249** (1985) 557–592.
- [63] C. L. Wainwright, *CosmoTransitions: Computing Cosmological Phase Transition Temperatures and Bubble Profiles with Multiple Fields*, *Comput. Phys. Commun.* **183** (2012) 2006–2013, [[arXiv:1109.4189](#)].
- [64] V. Guada, M. Nemevšek, and M. Pintar, *FindBounce: Package for multi-field bounce actions*, *Comput. Phys. Commun.* **256** (2020) 107480, [[arXiv:2002.00881](#)].
- [65] S. R. Coleman, *The Fate of the False Vacuum. 1. Semiclassical Theory*, *Phys. Rev. D* **15** (1977) 2929–2936. [Erratum: *Phys.Rev.D* 16, 1248 (1977)].
- [66] G. W. Anderson and L. J. Hall, *The Electroweak phase transition and baryogenesis*, *Phys. Rev. D* **45** (1992) 2685–2698.
- [67] B. Gripaios, A. Pomarol, F. Riva, and J. Serra, *Beyond the Minimal Composite Higgs Model*, *JHEP* **04** (2009) 070, [[arXiv:0902.1483](#)].
- [68] A. Angelescu, F. Goertz, and A. Tada, *Z_2 Non-Restoration and Composite Higgs: Singlet-Assisted Baryogenesis w/o Topological Defects*, [arXiv:2112.12087](#).
- [69] J. Preskill, S. P. Trivedi, F. Wilczek, and M. B. Wise, *Cosmology and broken discrete symmetry*, *Nucl. Phys. B* **363** (1991) 207–220.
- [70] S. A. Abel, S. Sarkar, and P. L. White, *On the cosmological domain wall problem for the minimally extended supersymmetric standard model*, *Nucl. Phys. B* **454** (1995) 663–684, [[hep-ph/9506359](#)].
- [71] C. Chatterjee, M. Kurachi, and M. Nitta, *Topological Defects in the Georgi-Machacek Model*, *Phys. Rev. D* **97** (2018), no. 11 115010, [[arXiv:1801.10469](#)].
- [72] M. Eto, M. Kurachi, and M. Nitta, *Non-Abelian strings and domain walls in two Higgs doublet models*, *JHEP* **08** (2018) 195, [[arXiv:1805.07015](#)].
- [73] U. A. Yajnik, H. Widyana, D. Choudhari, S. Mahajan, and A. Mukherjee, *Topological defects in the left-right symmetric model and their relevance to cosmology*, *Phys. Rev. D* **59** (1999) 103508, [[hep-ph/9812406](#)].
- [74] R. Jeannerot, J. Rocher, and M. Sakellariadou, *How generic is cosmic string formation in SUSY GUTs*, *Phys. Rev. D* **68** (2003) 103514, [[hep-ph/0308134](#)].
- [75] G. Lazarides, M. Reig, Q. Shafi, R. Srivastava, and J. W. F. Valle, *Spontaneous Breaking of Lepton Number and the Cosmological Domain Wall Problem*, *Phys. Rev. Lett.* **122** (2019), no. 15 151301, [[arXiv:1806.11198](#)].
- [76] J. Chakraborty, R. Maji, and S. F. King, *Unification, Proton Decay and Topological Defects in non-SUSY GUTs with Thresholds*, *Phys. Rev. D* **99** (2019), no. 9 095008, [[arXiv:1901.05867](#)].